Organic Electronics 56 (2018) 139–145

Contents lists available at ScienceDirect

Organic Electronics

journal homepage: www.elsevier.com/locate/orgel

All-printed full-color pixel organic photodiode array with a single active layer

Igal Deckman, Pierre Balthazar Lechêne, Adrien Pierre, Ana Claudia Arias*

Electrical Engineering and Computer Sciences, University of California Berkeley, Berkeley, CA 94720, USA

ARTICLE INFO

Keywords:
Flexible electronics
Organic photodetectors
Organic photodiodes
Full-color photodiodes
Printed electronics

ABSTRACT

A new fabrication method to realize fully-printed organic photodiode (OPD) arrays capable of RGB light separation is presented. From the photocurrents generated by each pixel type under the light from RGB LEDs, we demonstrate that this "White", "Yellow" and "Red" array can successfully detect and reconstruct colors in the RGB system, with an average accuracy of 98.5%. A flexible broadband OPD array is printed on PEN substrate by blade-coating PEDOT:PSS, a polyethylenimine cathode interlayer and the photo-active layer, and screen-printing on top a patterned PEDOT:PSS anode. The OPD array achieves an average EQE of ~37% at −4 V bias over the whole visible spectrum, 5 orders of magnitude of linear dynamic range (LDR), a 0.5 nA/cm^2 dark current, and maintains these performances in ambient conditions for more than 30 h. Pixels detecting "White", "Yellow" and "Red" are fabricated by spray-coating two color filters. The substrate is used as a separator between the filters and OPD array. This physical separation allows solution processing of the filters regardless of their electrical properties or of the compatibility of their solvents with the OPD, thus broadening the choice of filter materials while offering a simple fabrication process. The combination of broadband OPD and broadband filters used in this configuration can significantly simplify the fabrication of spectrally-selective photosensors and full-color imagers.

1. Introduction

Today, there is a growing interest for optical systems that offer spectral selectivity and multi-color detection as these properties are key requirements for a variety of applications such as color detectors and imagers, chemical and biological optical sensors, multi-wavelength visible light communication systems and optical-medical sensors [1–3]. Spectral selectivity in conventional color imagers is typically achieved by combining broadband silicon photodiodes (PDs) and Bayer Color Filter Arrays (CFA), which consist of a mosaic of red (R), green (G) and blue (B) color filters with minimal spectrum overlap. Today organic photodiodes (OPDs) can't compete with resolution (pixel size < 1.2 μm) of silicon-based PD. However, OPDs offer mechanical flexibility, lightweight, spectral tunability, low-cost solution processing over large areas which are beneficial for applications that require low light intensity operation, large area and flexibility, in addition the performance of OPDs are comparable to silicon PD [4]. OPDs have proven to be a great alternative to their inorganic counterparts in the fields of Internet of Things (IoT), wearable and disposable devices [5–11]. However, realization of spectral selectivity and multi-color detection in a tunable manner without deteriorating the OPD's performance, mechanical flexibility or fabrication advantages is still an open challenge. Color detection can be achieved with a photodiode array able to detect an independent base of the color space that will subsequently be re-constructed in the RGB base. The utilization of an alternative CFA made of printable organic compounds could be a complementary solution for multi-color flexible OPDs.

Today the mainstream approach to realize spectral selectivity in OPDs is focused on the modification of either the composition or the thickness of the photoactive layer. This approach is limited by fabrication methods, materials performance and availability. The strategy of composition modification consists in using narrowband materials for the active layer to tune its optical absorption exclusively to the region of interest. This requires that both the donor and acceptor materials absorb only in the desired wavelength range, since absorption by any of these two entities leads to photoresponse. The limited availability of narrowband absorbing acceptors, especially in the red and green spectrum regions is the main challenge [1]. In addition, this strategy also requires the prevention of inter-mixing of active layers between adjacent pixels. Typically, in organic electronics mixing is avoided by the utilization of orthogonal solvents or by thermal evaporation of subsequent layers or pixels. The number of layers required in a multi-

* Corresponding author.
E-mail address: acarias@berkeley.edu (A.C. Arias).

https://doi.org/10.1016/j.orgel.2018.02.009
Received 9 November 2017; Received in revised form 5 February 2018; Accepted 8 February 2018
Available online 10 February 2018

color array detector is high and the orthogonal solvent technique is limited [12]. On the other hand, evaporation can be used for low molecular weight molecules further reducing the materials choice [13,14]. The second strategy in the active layer modification approach is based on device optics engineering. The active layer positioned between the substrate's semi-transparent conductive oxide and the completely reflective metal electrode forms a low-finesse cavity where light absorption is governed by the cavity mode(s) [15]. Changing the cavity length by tuning the thicknesses of the semi-transparent electrode [16] or of the active layer [17], can narrow the OPD spectral response. The main drawbacks of the optical cavity approach for actual sensors are: i) poor control of the selectivity due to the strong - and difficult to fine-tune - influence of the active layer on the optical properties; ii) a strong angular dependence of the spectral response and iii) the necessity of highly reflective electrodes. Realization of multi-color arrays by this strategy requires deposition of pixels with a wide variety of thicknesses, which introduces fabrication challenges as described for the narrow-band materials strategy. Thus, today the active layer modification approach is suitable to tune single-color OPDs but it is not compatible with printed multi-color OPD arrays.

Another approach for realizing spectral selectivity in OPDs is the utilization of a broadband absorbing active layer in combination with optical filters, a strategy adopted with inorganic PD [18]. This approach benefits from the availability of broadband absorbing materials already well optimized for organic solar cells, and from the simplicity of single-active-layer OPD array fabrication. Yu et al. were the first to achieve selective spectral responses by placing sequentially R,G and B monocolor filters above the same linear OPD array [19,20]. Later Higashi et al. realized a red-light photodetector by combining a filter and a broadband OPD in one device [21]. It was done by thermal evaporation of a CuPc/C60 bilayer above the blue and green light filters, α,ω-diphenyl-sexithiophene (P6T) and α,ω-bis(biphenyl-4-yl)-ter-thiophene (BP3T) respectively, that also played the role of the anode. In this configuration where the filter is a part of the OPD electrode, the filter materials have to be compatible in terms of roughness, adhesion and immiscibility for the following deposition of the active layer. In addition, the filter materials also have to combine good charge transport as an electrode, the desired optical window as a filter, with exciton-blocking capability to prevent the generation of parasitic photocurrent. These requirements significantly narrow the choice of filter materials. In addition, the realization of multi-color OPD arrays in this configuration faces the fabrication challenge of the potential mixing of the filters of adjacent pixels. Thus, the limited availability of electrode compatible filter materials and the filter fabrication challenges inhibit the widespread use of multi-color OPD arrays based on broadband absorbing OPDs and optical filters. However, the simplicity of fabrication of the single-active-layer OPD array highlights the need for a new OPD-filter configuration that can be fabricated by low-cost solution processing and compatible with a variety of filter and active layer materials.

Here, we achieve the first flexible, full-color, all printed 2D OPD array by using a new approach of combining a single-active-layer fully-printed broadband OPD and two wide range absorbing printed filters. In our approach the substrate is used as a separator between the filters and OPD array to form pixels that detect Red, Yellow and White light. This physical separation allows solution processing of the filters regardless of their electrical properties or of the compatibility of their solvents with the OPD, thus broadening the choice of filter materials while offering a simple fabrication process. The use of the same broadband OPD, compatible with printing techniques, significantly simplifies the array fabrication processing. Conventional RGB color detectors use three narrow-band filters to detect specific regions of the light spectrum. We combine only two broadband filter materials and demonstrate arrays that successfully detect light generated by the RGB color-scheme. The materials used for the filters, [N-9′-heptadecanyl-2,7-carbazole-alt-5,5-(4′,7′-di-2-thienyl-2′,1′,3′-benzothiadiazole)] (PCDTBT) and Poly (9,9-dioctylfluorene-alt-benzothiadiazole) (F8BT):PC60BM, gradually reduce the absorption window of the as-printed OPD. In our arrays, as-printed non-filtered OPD pixels absorb over the whole visible range, from 350 to 750 nm, and are referred to as “White” (W) pixels. The deposition of a F8BT:PC60BM layer as a filter narrows the photoresponse window to the range of 500–750 nm, thus forming a “Yellow” (Y) pixel. “Red” (R) pixels are achieved when PCDTBT is added to the F8BT:PC60BM filter, resulting in a photoresponse window from 600-750 nm. We demonstrate that the measurement of the photocurrents from the RYW pixels exposed to controlled RGB-colored light can be used to successfully identify and reconstruct the RGB composition of the light, with an accuracy above 95%. Thus, we show that the combination of “white”, “yellow” and “red” pixels based on the broadband OPD and two broadband filters allows to realize flexible all-printed full-color OPD arrays.

2. Results

The OPD array was fabricated using a combination of blade coating and screen printing techniques on a flexible polyethylene naphthalate (PEN). Blade-coating allows to controlled deposition of layers of thin films (tens of nanometers) with a high uniformity, while screen-printing allows deposition of patterned thicker layers films (microns). Blade-coating was used to deposit all thin film layers of the OPDs while and the top electrode (the last layer) was screen-printed, thus allowing the patterning of the pixel array. Fig. 1a illustrates the different steps of the fabrication process. We overcame the lack of air/humidity stable low work-function printable cathode by utilization of a cathode interlayer and inverted device architecture. To fabricate the bottom cathode, a layer of poly(3,4-thylenedioxythiophene): poly(styrenesulfonate) (PEDOT:PSS) was blade-coated on the PEN substrate, followed by the deposition of the electron selective interlayer ethoxylated polyethylenimine (PEIE). Then, the donor-acceptor blend composed of PVD4650:PC70BM (1:2) was uniformly deposited on top of the PEIE to form the active layer. Finally, the pixel area and pixels array geometry were defined by screen-printing the patterned PEDOT:PSS anode. Thus, an all-printed two-dimensional OPD array (32 × 32 pixels 1 × 1 mm each pixel) was fabricated on an ITO-free flexible plastic substrate as shown in Fig. 1b. The PCDTBT and F8BT:PC60BM (95:5 wt) filters were spray coated through shadow masks on the opposite side of the OPD array substrate in a mosaic pattern (see Supporting Information Fig. S1a). Utilization of the substrate as a separator between the OPD array and the filters allowed solution processing of the filters regardless of the orthogonality of their solvents with those used for the OPD materials.

The OPD performances are dictated by the charge generation and transport in the active layer as well as by the selectivity of the electrodes. The thickness of the active layer has been shown to influence dark current density and device yield, making it an important parameter to control. We previously demonstrated that high yield (the percentage of devices, which exhibit photodiode behavior) can be achieved with described printing methods for devices with active layer thickness above 570 nm [4]. To investigate the influence of the active layer's thickness on device performance, devices with 530, 840 and 1050 nm active layer thickness were fabricated by varying the blade coating speed and the active layer ink concentration. Representative current density–voltage (J–V) curves characteristic of the OPDs in dark and under a 550 nm 0.175 mW/cm^2 illumination are presented in Fig. 1c. The photocurrent density (J_{ph}) is relatively flat in the range of −2 to −5 V of reverse bias and in inverse relation to the active layer thickness, with values of 50, 36 and 35 μA (at −4 V) for 530, 840 and 1050 nm thick active layers respectively. The decrease of J_{ph} with increase of active layer thickness is related to an enhancement of charge recombination and space-charge effects in the thicker active layers [22,23]. The dark-current density (J_d) is 0.5 nA and constant in the range of −0.5 to −5 V for active layers thicker than 840 nm. The 530 nm active layer exhibits a continuous increase of J_d with increase of

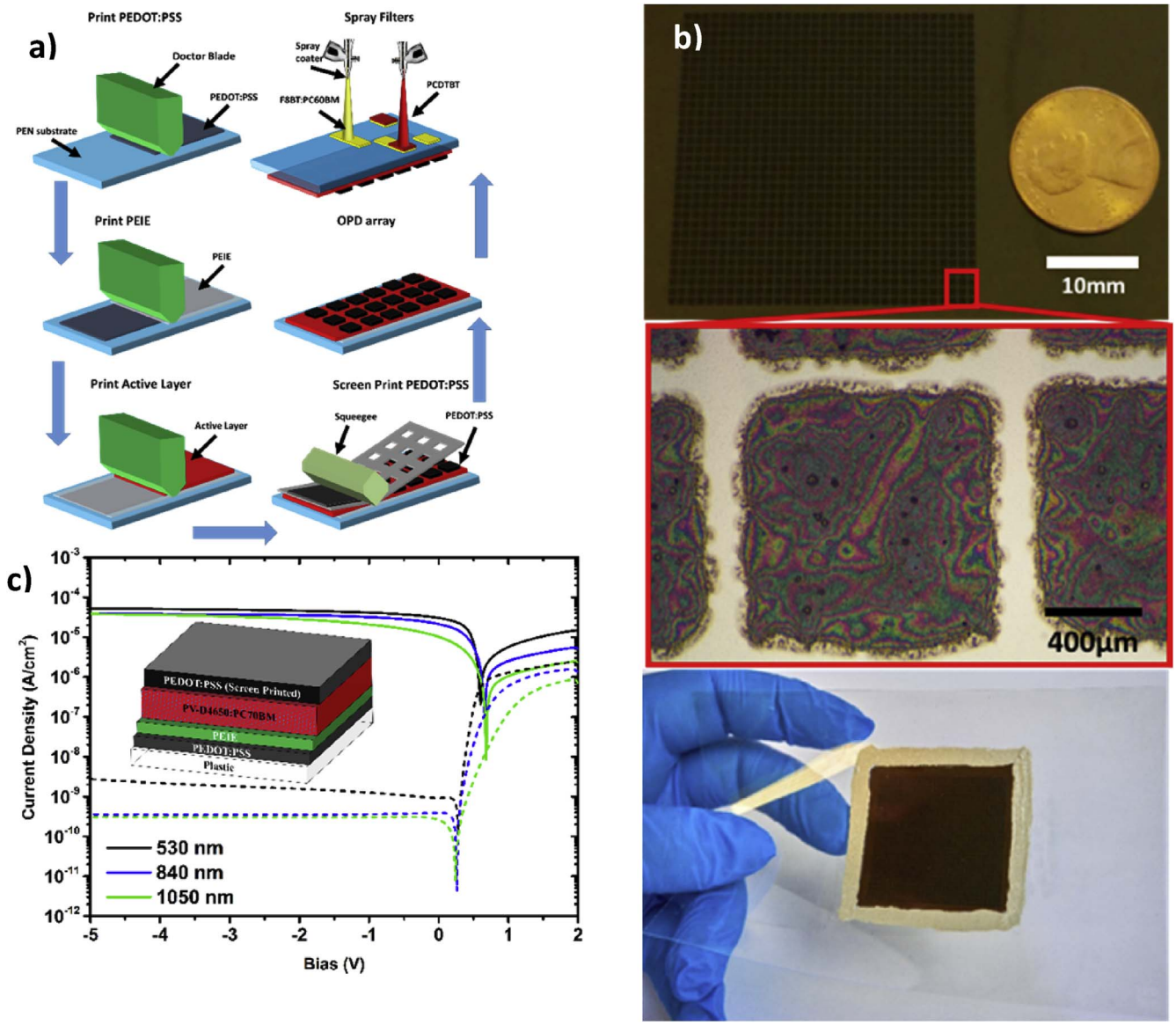

Fig. 1. a) Fabrication process of all-printed OPDs and filters deposition, b) Optical images of the 32 × 32 pixels OPD array with 1 × 1 mm pixels, c) Current density–voltage (J–V) characteristics of devices with 530, 840 and 1050 nm thick active layers in dark (dashed line) and under light conditions (solid line) at 532 nm and 0.175 mW/cm^2.

the reverse bias and reaches 1.4 nA/cm^2 at −4 V. The decrease of J_d with increase of active layer thickness can be explained by a higher shunt-resistance of the thicker layers [24,25]. The J_d of 0.5 nA/cm^2 is a relatively low value compared to recently reported state-of-the-art broadband and narrowband OPDs and it positively affects OPDs figures of merit, such as dynamic range, specific detectivity and power consumption [1,21,26–29]. Thus, active layer thickness leading to a minimal J_d should be preferred, and since the J_{ph} of the 840 nm thick layer is higher than the 1050 nm one, then 840 nm can be considered as the optimal thickness of the active layer. In addition, the array with 840 nm thick active layer has the lowest deviation in performance as shown by J-V curves of 12 pixels from different parts of the array (see Supplementary Information Fig. S2b). Since, the blade coated PEDOT:PSS/PEIE cathode and screen printed PEDOT:PSS anode were already optimized and fully characterized in our previous work [4], the devices can be considered as optimized and will be used for all subsequent experiments.

The linear dynamic range (LDR) of the OPDs was characterized at three wavelengths (660, 525 and 465 nm) to cover the whole visible spectrum and the resulting J_{ph} at −4 V is presented in Fig. 2a. The difference between light intensity at J_d and at upper limit of linearity demonstrated by OPDs for all three wavelengths is over five orders of magnitude. The upper limit of linearity in OPDs with printed non-metal top electrode is limited by conductivity and stability of the electrode in contrast to OPDs with evaporated metal electrode where the limit is defined by bimolecular recombination of the photogenerated charge carriers [30]. As a result, the demonstrated LDR is much lower in comparison to OPDs with evaporated top electrode and is typical to previously reported all-printed OPDs [1,4,31]. The OPD exhibits −3 dB cut-off frequencies of 0.5, 0.8 and 1.1 kHz at 1, 3 and 5 V reverse bias voltage respectively Fig. 2b. These cut-off frequency values are ~2 orders of magnitude lower compared to previously reported OPDs with evaporated top metal electrode and are typical to all-printed OPDs [1]. The non-linear increase of the cut-off frequency with applied bias and previously shown discrepancy in frequency response for similar devices with non-metal and aluminum cathodes indicate that inefficient carrier extraction at printed electrodes could be a limiting factor for the all-printed OPDs [1,2,4,32]. It is also noteworthy that it was previously shown that devices with higher charge extraction at the electrodes have higher J_d leading to lower detectivity [4]. Another key factor in OPDs

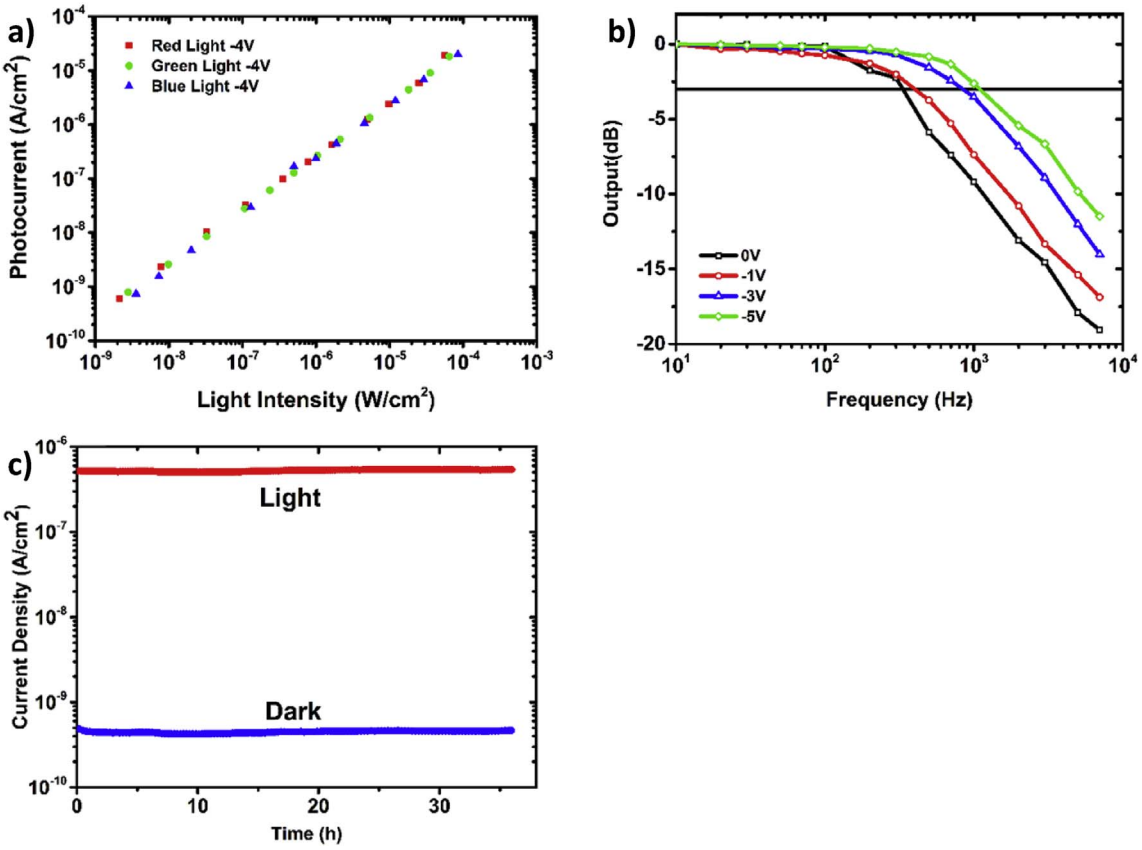

Fig. 2. Dynamic response of the OPD at 630, 525 and 465 nm biased at −4 V (a), frequency response of the OPD under 525 nm sine-modulated light at various biases (b), OPD biased continuously at −4 V for 36 h in air alternating between light (525 nm) and dark with a 50% duty cycle (c).

performance is their stability. To quantify stability, the OPDs were continuously biased at -4 V for 36 h while being exposed to alternating dark and light conditions (50% duty cycle at 20 mHz frequency) with a light wavelength in the middle of their sensing range (525 nm) Fig. 2c. The stability tests were performed in air without adding encapsulating layers to the device structures and were consistent with the conditions used for all device characterization reported here. It can be seen that during the 36 h period the OPD exhibit a stable performance with J_d of $4.5 \pm 0.1 \times 10^{-10}$ A/cm^2 and J_{ph} of $5.25 \pm 0.13 \times 10^{-7}$ A/cm^2. To summarize, the OPD demonstrates stable performances at the ambient conditions comparable with recently reported state of the art all-printed OPDs [1,4].

As a first step of the spectral response characterization, the absorbance of active layer was measured. Fig. 3a demonstrates that the active layer consisting of PVD4650:PC70BM has a broad absorbance in the range of 350–800 nm with the main peaks at 375, 470, 555 and 630 nm, the last two appearing as shoulders. As a result the typical external quantum efficiency (EQE) spectrum of the non-filtered OPDs shown in Fig. 3b (blue line) exhibits the same broad spectral response between 350 and 750 nm with similar to absorbance spectra features. The best pixels demonstrate an average EQE as high as 57% over the visible spectrum (between 380 and 700 nm) (as shown in Supplemental Information Fig. S1b), but the typical array pixel had an average EQE of 37% at −4 V bias. That value is higher than those in single-component active-layer OPDs and similar to broadband BHJ based OPDs [4,26–28,33]. These results demonstrate that the OPD covers the whole visible spectrum with EQE variations of 7% over this range, which makes it a good candidate for spectrally broadband applications [23,24].

To characterize spectral selectivity of the OPD array EQE of filter combined OPDs was measured. To prevent confusion the non-filtered OPDs are hereinafter referred to as “white”, while the OPDs with spray coated an absorbing filter of F8BT:PC60BM (95:5 wt%) are called “yellow” and the OPDs with PCDTBT and F8BT:PC60BM filters, are called “red” OPDs. The absorption spectrum of F8BT:PC60BM (Fig. 3a) demonstrates a step-like absorption coefficient (α) for wavelengths < 520 nm, with tail decreasing linearly from 0.15α to 0 in the range of 530–850 nm. 5 wt% of PC60BM was added to F8BT in order to quench photoluminescence from F8BT, which would induced parasitic photocurrent at wavelengths < 500 nm (see Supplementary Information Fig. S3) [34]. The EQE spectrum of the “yellow” OPD is ~5% lower than that of the “white” OPD in the range of 800 to 530 nm: it has a sharp drop between 530 nm and 500 nm followed by zero photoresponse for wavelengths below 500 nm. (Fig. 3b). The 5% shift originates from the linear tail (530–800 nm) in the absorption spectrum of F8BT:PC60BM that reduces light intensity in the region, whereas the absence of photoresponse at wavelengths < 500 nm comes from the main absorption peak of F8BT. The EQE does not show a parasitic photoresponse in the blue region, generally related to the electron acceptor absorption, and its value is comparable to previously reported green-light-selective BHJ based OPDs that are characterized by much higher J_d [26,33]. In contrast to the “white” OPD, the “yellow” OPD demonstrates sensitivity only in the range of 500–750 nm, responsible for the green and red parts of the visible spectrum. The absorption spectrum of PCDTBT (Fig. 3a) is characterized by two broad peaks at 390 and 550 nm and it covers the visible range till 650 nm, which is approximately 100 nm less than the range covered by the PV-D4650:PC60BM active layer. The valley between the peaks is located in the middle of the main F8BT peak, therefore a superposition of these two filters, with appropriate relative thicknesses, gives a flat step-like absorption (see Supplementary information Fig. S2a). As a result of the PCDTBT and F8BT:PC60BM filtering, the EQE spectrum of the “red” OPD (Fig. 3b) shows a peak of 27% at 670 nm and a 60 nm breadth (FWHM). The obtained EQE and FWHM values are similar to previously reported

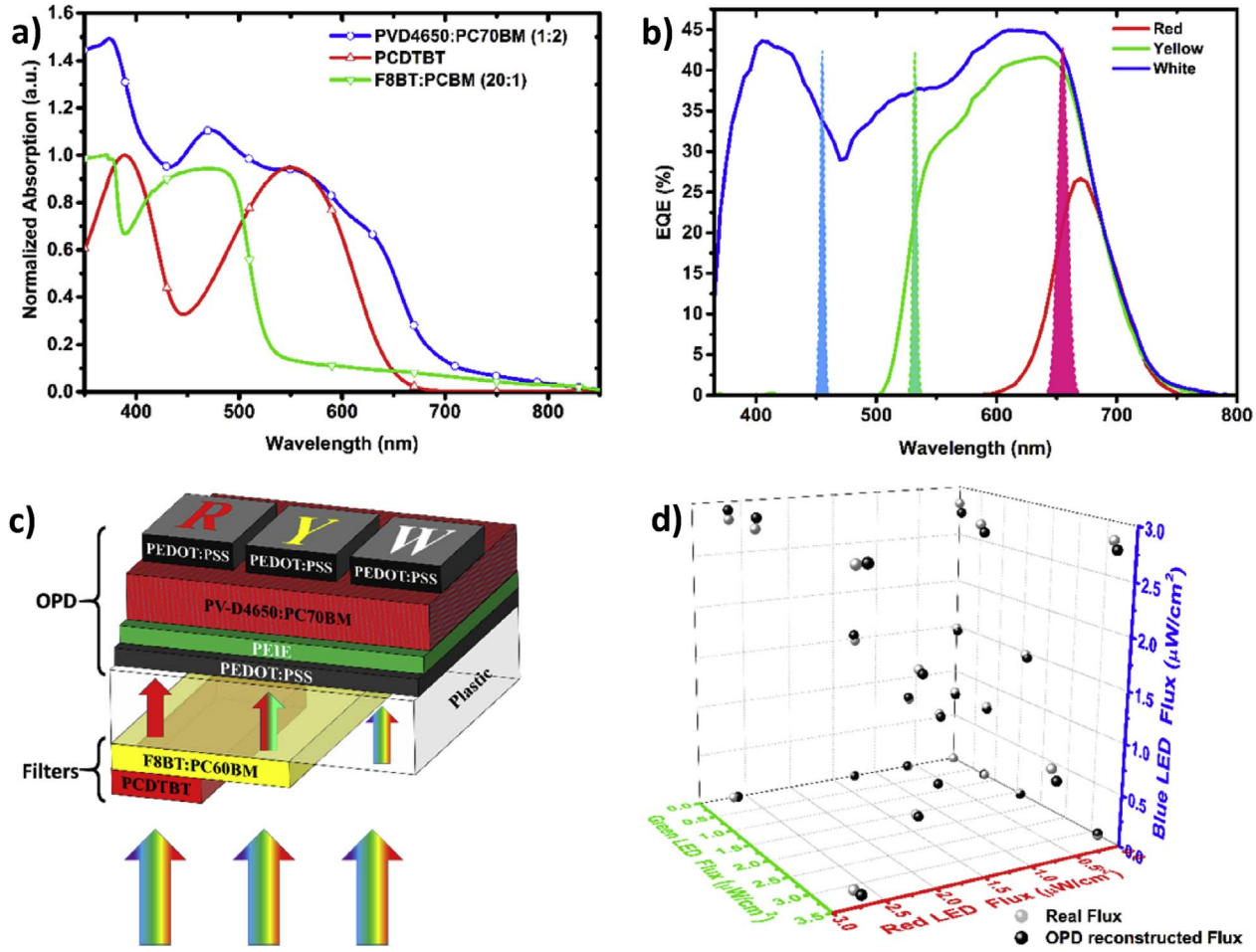

Fig. 3. Absorption spectra of PCDTBT, F8BT:PC60BM and PV-D4650:PC70BM (1:2) thin films (a), EQE of "white", "yellow" and "red" OPDs at −4 V bias and LEDs emission spectra (b), OPDs cross section and general concept of color separation (c), RYW reconstructed and real LED flux (d). (For interpretation of the references to color in this figure legend, the reader is referred to the Web version of this article.)

narrowband red-light-selective OPDs [21,28]. So, in contrast to "white" and "yellow" OPDs the "red" one demonstrates sensitivity in a much narrow range of 600–750 nm, responsible for the red part of the visible spectrum. Thus, by using the same all-printed broadband active layer OPD array combined with substrate-separated spray coated absorption filters, we succeeded to gradually narrow the OPDs photoresponse from 350-750 nm for a detection of "white" light, to 500–750 nm for "yellow" light sensitive OPD, and to 600–750 nm for "red" sensitive OPDs.

To evaluate the color selectivity capabilities of the OPD array combined from filtered and non-filtered pixels we examined the position and overlap of their photoresponse spectra. A Red Yellow White (RYW) OPD array is fabricated and consists of the "red", "yellow" and "white" pixels described above. In this array, the "red" pixel has a narrowband EQE, with a peak at 670 nm and a FWHM of 60 nm (645–705 nm). The "yellow" pixel has a broader photo-response window, with a flat peak of ~41% across the 600 nm to 655 nm region and a FWHM of 160 nm (530–690 nm). As a result, the "yellow" pixel completely covers the absorption range of the "red" pixel and covers an additional 115 nm with high response values (530–645 nm), thus covering both the red and green region of the light spectrum. Finally the "white" OPD has a photo-response covering the whole visible spectrum. It has two peaks, with highest EQE values of 43.6% (at 405 nm) and 45% (620 nm), and the trough between them has a minimum value of 29% (470 nm). Therefore, the "white" OPD can be considered to have a FWHM of 315 nm (370–685 nm), enough to detect light across this whole range, even if the photo-response is not homogeneous. As a result, it absorbs the Red, Green and Blue components of RGB light source. The RYW OPD array therefore consists of three pixels that can detect three gradually inclusive combinations of R, G and B light: the "red" pixel absorbs only the red part, the "yellow" pixel absorbs red and green, while the "white" pixel absorbs all three components. The EQE of "yellow" pixels (~35%) is similar to recently reported narrowband green OPDs (~40%) [33] while the EQE of "red" pixels (~25%) is slightly lower in comparison to state-of-the-art red OPDs (~34%) [29]. Thus, despite the EQE decrease due to filters incorporation the pixels' performance is still comparable with state-of-the-art narrowband OPDs.

It has been shown that detectors with 100 nm of FWHM can provide good color discrimination, even with some overlap of the absorption ranges, if the absorption peaks are at least more than 60 nm apart [35]. The three pixels indirectly satisfy the 100 nm of FWHM criterion for specific color detection: the "red" pixel has a FWHM of 60 nm, the "yellow" pixel half-maximum zone covers 115 nm specifically for the green light and the "white" pixel has an additional 160 nm (370–530 nm) of specific range for the blue light. The general principle of RGB space reconstruction from the RYW photocurrent measurements can be formulated as: red light is sensed with the "red" pixel, green is obtained by subtracting the photoresponse of the "red" pixel from that of the "yellow" pixel, and blue light is reconstructed by subtracting the photoresponse of the "yellow" from that of the "white" pixel (Fig. 3c). The proposed filters scheme is the simplest one from the fabrication prospective, since it relies on two filters and two chromophores only. When all others two filters schemes such as WGR, WBR or WBR require at least two chromophores and stencil for each bandpass/bandstop

Table 1
Photoresponse matrix elements.

	Red LED	Green LED	Blue LED
EQE of Red OPD	0.186	0	0
EQE of Yellow OPD	0.394	0.256	0
EQE of White OPD	0.423	0.444	0.391

filter.

To quantitatively demonstrate that the RYW array can specifically sense the RGB color space, the individual responses of the R, Y and W pixels to variable RGB colored light sources are measured and compiled as a photoresponse matrix as shown in Table 1. The variable RGB light source is composed of red, green and blue LEDs (respective wavelengths: 630, 525 and 465 nm, as indicated by the colored peaks on Fig. 3b), each with three different flux intensities that cover the whole LDR of the OPD. Every element M_{ij} of the photoresponse matrix is the EQE average value of 5 pixels of same type i (R,Y or W) measured for the LED source j (R,G or B). The matrix values are in good agreement with values previously obtained from the EQE spectra. The matrix respects the following equation:

$$\begin{pmatrix} C_R \\ C_Y \\ C_W \end{pmatrix} = (EQE_{i,j}) \begin{pmatrix} F_r \\ F_g \\ F_b \end{pmatrix} \quad (1)$$

where C_i is the current generated by the OPD pixel i (R, Y or W) and F_j is the flux of the light coming from the LED j (R, G, or B). The matrix has a rank of 3 and can be diagonalized and inverted, indicating that the RYW array properly detects an independent base of the RGB color space. Therefore, any combination of RGB light gives rise to a unique combination of RYW OPD currents and can be identified from them. This approach is not limited to specific RGB light only. Lights constructed from any combination of base colors could be successfully recognized as long as the base colors result in an invertible photoresponse matrix. To calculate the flux of the RGB LEDs from the current values generated by the OPDs, Eq. (1) simply needs to be inverted:

$$\begin{pmatrix} F_r \\ F_g \\ F_b \end{pmatrix} = (EQE_{i,j})^{-1} \begin{pmatrix} C_R \\ C_Y \\ C_W \end{pmatrix} \quad (2)$$

As an experimental verification, OPD measurements of colored lights created with varying combinations of RGB LEDs are performed. From the photocurrent measured from each OPD pixels and the inverted photoresponse matrix, the composition of the lights are reconstructed and compared to the original input. The results are given in Fig. 3d, which shows the composition of colored lights as a function of their RGB coordinates, as they were inputted (real flux measured by calibrated silicon photodiode) and reconstructed from the OPD measurement (OPD reconstructed flux). The average error between the real and reconstructed light compositions is 2.6% of the light's intensity (calculated as the distance between the real and reconstructed points in the RGB space relative to the position of the real point in this space). The identification of lights composed from only one LED source (points situated on the axis of the graph) is the most accurate as it relates directly to the photoresponse matrix, with an average error of 1.5%. In particular, detection of the green LED alone and of the red LED alone consistently yields the lowest error (0.3% in both cases), while identification of the blue LED only is the most error prone with maximum error of 3.9%. In our system blue LED light is detected only by the "white" pixel, whereas the green LED light is detected by the "white" and "yellow" pixels and the red LED light is detected by all three pixels (see Fig. 3b). As a result, the photoresponse matrix and its inverse are lower triangle matrices (see Table 1). Therefore, the increased error in flux reconstruction of individual blue light source is result of multiplication of nonzero matrix elements by parasitic photocurrents generated in "red" and "yellow" pixels. Compounded lights, mixing two or three LEDs with various intensities yield an average error of 3.2%. The maximum error is 4.4% and occurs for a light composed of the three RGB LEDs, all at medium intensity. In general, the reconstruction error tends to be higher for lights composed of the three RGB components at medium or high intensities. Nonetheless, for each colored light, the input and the reconstructed values remain close enough that identification of the reconstructed lights are unequivocal. Therefore, the all-printed RYW OPD array is able to identify colored light and its intensity encoded in the RGB system with accuracy of > 95.5%.

3. Conclusion

In conclusion, we developed for the first time an all-printed full-color 2D OPD array. It is based on a broadband OPD and two spray coated organic filters. The all-printed OPD is characterized by stable performances in ambient conditions, EQE averaging ~37% over the whole visible spectrum, 5 orders of magnitude of LDR and 0.5 nA/cm^2 dark current. We presented a new filter-OPD configuration where the substrate was used as a physical separator between the OPD array and the filters. The advantage of this separation is that the filter materials can be chosen purely on their optical properties and can be solution-processed without interfering with the OPD fabrication. The chosen broadband filters allowed to gradually narrow the photoresponse of OPD pixels from 350-750 nm for a no-filtered "white" OPD, to 530–750 nm for a "yellow" OPD, and to 600–750 nm for a "red" OPD. These three types of OPDs were integrated into a RYW OPD pixel array. From the photocurrents generated by each pixel type under the lights from RGB LEDs, we demonstrated that this RYW array could successfully detect and reconstruct colors in the RGB system, with an average accuracy of 98.5% (the lowest accuracy was 95.5%). The OPD pixel size fabricated by the proposed technique can be scaled down to a screen printing resolution limit that today is 20–40 μm [36]. Printing fabrication techniques are also suitable for the fabrication of large area OPD arrays or large individual pixels. The proposed filter-OPD configuration and the combination of broadband OPD and broadband filters can significantly simplify the fabrication of spectral-selective photosensors and full-color imagers.

4. Experimental section

4.1. Printed devices

Polyethylene naphthalate (PEN) from Teijin films was used as substrates for the OPDs. A 50 W plasma was applied through a stencil to define a central hydrophilic area for PEDOT:PSS (Orgacon IJ-1005) blade coating at 1.6 cm/s with a 200 μm gap, using a Zehntner ZUA 2000 blade coater, followed by thermal annealing for 10 min at 120 °C. The samples were then transferred to a nitrogen glove box where PEIE (0.4 wt% solution in 2-methoxyethanol) (Sigma-Aldrich) was coated onto PEDOT:PSS at 1.6 cm/s with a 100 μm gap then annealed for 10 min at 100 °C. A PV-D4650 (Merck KGaA, Darmstadt, Germany):PC71BM (Solaris Chem) (1:2 wt) solution dissolved to 60 mg/ml in chlorobenzene was blade coated on a 40 °C platform at 2.8 cm/s with a 200 μm gap followed by 120 °C for 10 min annealing. The sample was plasma treated (50 W for 3s) right before screen printing of the top PEDOT:PSS (Orgacon EL-P 5015) electrode array (32 × 32 pixels of 1 mm^2 area each) at 10 cm/s using an ASYS ASP 01M screen printer. Devices were dried out under vacuum for ten minutes before annealed in a glove box at 120 °C for 5 min. The filters were deposited by airbrushing method form 15 mg/ml solutions in chlorobenzene through a Kapton stencil beforehand adhered to the PEN substrate.

4.2. Device characterization

The film thickness were measured with Veeco 6M Dektak profilometer. Devices characterization was performed with Agilent B1500a semiconductor device parameter analyzer in shielded probe station to ensure a dark and low-noise environment. External quantum efficiency (EQE) were measured with a PV Measurements QEXL system. An Electro Optical Components DHPCA-100 trans-impedance amplifier and Analog Discovery 100MSPS USB Oscilloscope were used for frequency measurements. The RGB light source was made from red (630 nm), green (525 nm) and blue (465 nm) LEDs. Hamamatsu S2387-66R calibrated silicon photodiode was used to measure LED flux.

Acknowledgements

This work was supported in part by Merck KGaA, Darmstadt, Germany, NSF Graduate Fellowship Research Program under Grant No. DGE-1106400 and Grant No.1610899. Portions of this work were performed as a User project at the LBNL Molecular Foundry. Work at the Molecular Foundry was supported by the Office of Science, Office of Basic Energy Sciences, of the U.S. Department of Energy under Contract No. DE-AC02-05CH11231. The authors acknowledge Dr. Toby Cull, Dr. Lichun Chen and Dr. Andromachi Malandraki for discussion on the materials processing and device fabrication.

Appendix A. Supplementary data

Supplementary data related to this article can be found at http://dx.doi.org/10.1016/j.orgel.2018.02.009.

References

[1] R.D. Jansen-van Vuuren, A. Armin, A.K. Pandey, P.L. Burn, P. Meredith, Organic photodiodes: the future of full color detection and image sensing, Adv. Mater. 28 (24) (2016) 4766–4802.
[2] K.J. Baeg, M. Binda, D. Natali, M. Caironi, Y.Y. Noh, Organic light detectors: photodiodes and phototransistors, Adv. Mater. 25 (31) (2013) 4267–4295.
[3] W. Li, S. Li, L. Duan, H. Chen, L. Wang, G. Dong, Z. Xu, Squarylium and rubrene based filterless narrowband photodetectors for an all-organic two-channel visible light communication system, Org. Electron. 37 (2016) 346–351.
[4] A. Pierre, I. Deckman, P.B. Lechêne, A.C. Arias, High detectivity all-printed organic photodiodes, Adv. Mater. 27 (41) (2015) 6411–6417.
[5] S. Nau, C. Wolf, S. Sax, E.J.W. List-Kratochvil, Organic non-volatile resistive photoswitches for flexible image detector arrays, Adv. Mater. 27 (6) (2015) 1048–1052.
[6] T. Rauch, M. Boberl, S.F. Tedde, J. Furst, M.V. Kovalenko, G. Hesser, U. Lemmer, W. Heiss, O. Hayden, Near-infrared imaging with quantum-dot-sensitized organic photodiodes, Nat. Photon. 3 (6) (2009) 332–336.
[7] C.M. Lochner, Y. Khan, A. Pierre, A.C. Arias, All-organic optoelectronic sensor for pulse oximetry, Nat. Commun. 5 (2014).
[8] D. Li, X. Liu, G. Dong, L. Duan, D. Zhang, H. Zhao, L. Wang, Y. Qiu, A flexible blue light sensitive organic photodiode with high properties for the applications in low-voltage-control circuit and flexion sensors, Laser Photon. Rev. 8 (2) (2014) 316–323.
[9] T.N. Ng, W.S. Wong, M.L. Chabinyc, S. Sambandan, R.A. Street, Flexible image sensor array with bulk heterojunction organic photodiode, Appl. Phys. Lett. 92 (21) (2008) 213303.
[10] A. Nathan, A. Ahnood, M.T. Cole, L. Sungsik, Y. Suzuki, P. Hiralal, F. Bonaccorso, T. Hasan, L. Garcia-Gancedo, A. Dyadyusha, S. Haque, P. Andrew, S. Hofmann, J. Moultrie, C. Daping, A.J. Flewitt, A.C. Ferrari, M.J. Kelly, J. Robertson, G.A.J. Amaratunga, W.I. Milne, Flexible electronics: the next ubiquitous platform, Proc. IEEE 100 (Special Centennial Issue) (2012) 1486–1517.
[11] N. Kaur, S. Kumar, Colorimetric metal ion sensors, Tetrahedron 67 (48) (2011) 9233–9264.
[12] A.M. Gaikwad, Y. Khan, A.E. Ostfeld, S. Pandya, S. Abraham, A.C. Arias, Identifying orthogonal solvents for solution processed organic transistors, Org. Electron. 30 (2016) 18–29.
[13] P. Kovacik, G. Sforazzini, A.G. Cook, S.M. Willis, P.S. Grant, H.E. Assender, A.A. Watt, Vacuum-deposited planar heterojunction polymer solar cells, ACS Appl. Mater. Interfaces 3 (1) (2011) 11–15.
[14] K.P. Gritsenko, A.M. Krasovsky, Thin-film deposition of polymers by vacuum degradation, Chem. Rev. 103 (9) (2003) 3607–3650.
[15] L.A.A. Pettersson, L.S. Roman, O. Inganas, Modeling photocurrent action spectra of photovoltaic devices based on organic thin films, J. Appl. Phys. 86 (1) (1999) 487–496.
[16] K.H. An, B. O'Connor, K.P. Pipe, M. Shtein, Organic photodetector with spectral response tunable across the visible spectrum by means of internal optical microcavity, Org. Electron. 10 (6) (2009) 1152–1157.
[17] J.M. Lupton, R. Koeppe, J.G. Müller, J. Feldmann, U. Scherf, U. Lemmer, Organic microcavity photodiodes, Adv. Mater. 15 (17) (2003) 1471–1474.
[18] L. Frey, P. Parrein, J. Raby, C. Pellé, D. Hérault, M. Marty, J. Michailos, Color filters including infrared cut-off integrated on CMOS image sensor, Opt. Express 19 (14) (2011) 13073–13080.
[19] G. Yu, J. Wang, J. McElvain, A.J. Heeger, Large-area, full-color image sensors made with semiconducting polymers, Adv. Mater. 10 (17) (1998) 1431–1434.
[20] G. Yu, G. Srdanov, J. Wang, H. Wang, Y. Cao, A.J. Heeger, Large area, full-color, digital image sensors made with semiconducting polymers, Synth. Met. 111–112 (2000) 133–137.
[21] Y. Higashi, K.-S. Kim, H.-G. Jeon, M. Ichikawa, Enhancing spectral contrast in organic red-light photodetectors based on a light-absorbing and exciton-blocking layered system, J. Appl. Phys. 108 (3) (2010) 034502.
[22] A.J. Moulé, J.B. Bonekamp, K. Meerholz, The effect of active layer thickness and composition on the performance of bulk-heterojunction solar cells, J. Appl. Phys. 100 (9) (2006) 094503.
[23] M. Ramuz, L. Bürgi, C. Winnewisser, P. Seitz, High sensitivity organic photodiodes with low dark currents and increased lifetimes, Org. Electron. 9 (3) (2008) 369–376.
[24] D.M. Lyons, A. Armin, M. Stolterfoht, R.C.R. Nagiri, R.D. Jansen-van Vuuren, B.N. Pal, P.L. Burn, S.-C. Lo, P. Meredith, Narrow band green organic photodiodes for imaging, Org. Electron. 15 (11) (2014) 2903–2911.
[25] A. Armin, M. Hambsch, I.K. Kim, P.L. Burn, P. Meredith, E.B. Namdas, Thick junction broadband organic photodiodes, Laser Photon. Rev. 8 (6) (2014) 924–932.
[26] D.-S. Leem, K.-H. Lee, K.-B. Park, S.-J. Lim, K.-S. Kim, Y. Wan Jin, S. Lee, Low dark current small molecule organic photodetectors with selective response to green light, Appl. Phys. Lett. 103 (4) (2013) 043305.
[27] R.D. Jansen-van Vuuren, A. Pivrikas, A.K. Pandey, P.L. Burn, Colour selective organic photodetectors utilizing ketocyanine-cored dendrimers, J. Mater. Chem. C 1 (22) (2013) 3532.
[28] W. Li, D. Li, G. Dong, L. Duan, J. Sun, D. Zhang, L. Wang, High-stability organic red-light photodetector for narrowband applications, Laser Photon. Rev. 10 (3) (2016) 473–480.
[29] A. Armin, R.D. Jansen-van Vuuren, N. Kopidakis, P.L. Burn, P. Meredith, Narrowband light detection via internal quantum efficiency manipulation of organic photodiodes, Nat. Commun. 6 (2015) 6343.
[30] K. Maturová, S.S. van Bavel, M.M. Wienk, R.A.J. Janssen, M. Kemerink, Description of the morphology dependent charge transport and performance of polymer:fullerene bulk heterojunction solar cells, Adv. Funct. Mater. 21 (2) (2011) 261–269.
[31] F.P. García de Arquer, A. Armin, P. Meredith, E.H. Sargent, Solution-processed semiconductors for next-generation photodetectors, Nat. Rev. Mater. 2 (2017) 16100.
[32] S. Braun, W.R. Salaneck, M. Fahlman, Energy-level alignment at organic/metal and organic/organic interfaces, Adv. Mater. 21 (14–15) (2009) 1450–1472.
[33] S.J. Lim, D.S. Leem, K.B. Park, K.S. Kim, S. Sul, K. Na, G.H. Lee, C.J. Heo, K.H. Lee, X. Bulliard, R. Satoh, T. Yagi, T. Ro, D. Im, J. Jung, M. Lee, T.Y. Lee, M.G. Han, Y.W. Jin, S. Lee, Organic-on-silicon complementary metal-oxide-semiconductor colour image sensors, Sci. Rep. 5 (2015) 7708.
[34] S. Cook, Photo-induced Charge Generation and Recombination in Conjugated Polymer-methanofullerene Blend Films, Ph.D. Dissertation Imperial College, London, 2006.
[35] R. Jansen van Vuuren, K.D. Johnstone, S. Ratnasingam, H. Barcena, P.C. Deakin, A.K. Pandey, P.L. Burn, S. Collins, I.D.W. Samuel, Determining the absorption tolerance of single chromophore photodiodes for machine vision, Appl. Phys. Lett. 96 (25) (2010) 253303.
[36] W.J. Hyun, E.B. Secor, M.C. Hersam, C.D. Frisbie, L.F. Francis, High-resolution patterning of graphene by screen printing with a silicon stencil for highly flexible printed electronics, Adv. Mater. 27 (1) (2015) 109–115.